

Suppressing unknown disturbances to dynamical systems using machine learning

Juan G. Restrepo

Department of Applied Mathematics, University of Colorado at Boulder, Boulder, CO 80309, USA

Clayton P. Byers

Department of Engineering, Trinity College, Hartford, CT, 06106, USA

Per Sebastian Skardal

Department of Mathematics, Trinity College, Hartford, CT, 06106, USA

(Dated: October 10, 2023)

Identifying and suppressing unknown disturbances to dynamical systems is a problem with applications in many different fields. In this Letter, we present a model-free method to identify and suppress an unknown disturbance to an unknown system based only on previous observations of the system under the influence of a known forcing function. We find that, under very mild restrictions on the training function, our method is able to robustly identify and suppress a large class of unknown disturbances. We illustrate our scheme with the identification of unknown forcings to an analog electric chaotic circuit and with a numerical example where a chaotic disturbance to the Lorenz system is identified and suppressed.

Identifying and suppressing an unknown disturbance to a dynamical system is a problem with many existing and potential applications in engineering [1–9], ecology [10, 11], fluid mechanics [12–14], and climate change [15]. Traditional control theory disturbance identification and suppression techniques usually assume either an existing model for the dynamical system, linearity, or that the disturbance can be observed (for reviews of existing methods see, for example, Refs. [4, 16]). In this Letter we present a method for real-time disturbance identification and suppression that relies solely on observations of the dynamical system when forced with a known training forcing function. Our method is based on the application of machine-learning techniques to dynamical systems. Such techniques have found many applications, including the forecast of chaotic spatiotemporal [17] and networked [18] dynamics, estimation of dynamical invariants from data [19], control of chaos [20], network structure inference [21], and prediction of extreme events [22] and crises in non-stationary dynamical systems [23, 24]. For a review of other applications and techniques, see Refs. [25, 26]. In most of these previous works, a machine learning framework is trained to replicate the non-linear dynamics of the system based on a sufficiently long time series of the dynamics. In contrast, in this Letter we use machine learning to identify and subsequently suppress an unknown disturbance. Without knowledge of an underlying model for the dynamical system, and only based on observations of the system under a suitable known forcing function, our method allows us to reliably identify and suppress a large class of disturbances. Recent work [27] considers the problem of predicting the response of a system based on knowledge of the forcing (the disturbance) and the system’s response after training with known functions. That problem can be thought of as the “forward” problem, while the problem addressed here can be considered as the “inverse” problem. While both approaches are complementary, they apply to very

different situations. In addition to this fundamental difference, the main additional differences between our results and those of Ref. [27] are that we present a method to suppress the unknown forcing, that our method works for stochastic signals, and that we show that the training functions can be extremely simple (e.g., piecewise constant functions). We demonstrate our method with an experimental analog chaotic circuit and with numerical simulations.

Consider an N -dimensional dynamical system

$$\frac{d\mathbf{x}}{dt} = \mathbf{F}(\mathbf{x}) + \mathbf{g}(t), \quad (1)$$

where $\mathbf{x} \in \mathbb{R}^N$ is the state vector, $\mathbf{F} \in \mathbb{R}^N$ represents the intrinsic dynamics of the system, and $\mathbf{g}(t) \in \mathbb{R}^N$ represents an unknown (and usually undesired) disturbance. Our goal is to develop a scheme by which the disturbance can be identified and the system can be brought approximately to satisfy the undisturbed dynamics $d\mathbf{x}/dt = \mathbf{F}(\mathbf{x})$. We assume that we can observe the state vector \mathbf{x} , but we don’t need to assume knowledge of the intrinsic dynamics \mathbf{F} or the disturbance function \mathbf{g} . Assuming that we can force the system with a known *training forcing function* $\mathbf{f}(t)$, as

$$\frac{d\hat{\mathbf{x}}}{dt} = \mathbf{F}(\hat{\mathbf{x}}) + \mathbf{f}(t), \quad (2)$$

and observe $\hat{\mathbf{x}}(t)$ for a long enough time, our goal is to train a machine learning system to approximate $\mathbf{f}(t)$ given $\hat{\mathbf{x}}(t)$, and subsequently infer $\mathbf{g}(t)$ from observations of $\mathbf{x}(t)$ obtained from system (1). As we will show below, we find that we can recover a large class of forcing functions $\mathbf{g}(t)$ with very mild restrictions on the choice of training functions $\mathbf{f}(t)$. Once we infer $\mathbf{g}(t)$, we implement a self-consistent control scheme to suppress it from the dynamics. Our method works when the intrinsic dynamics are chaotic, periodic, or stationary.

Identification of the disturbance. First, we present our method for identifying the unknown disturbance $\mathbf{g}(t)$. We will illustrate our technique using reservoir computing, a type of machine learning framework particularly suited for dynamical systems problems [26]. In our implementation, we assume that we run system (2) during the “training” interval $[-T, 0]$, and collect a time-series of the observed state vector $\{\hat{\mathbf{x}}(-T), \hat{\mathbf{x}}(-T + \Delta t), \dots, \hat{\mathbf{x}}(0)\}$. These variables are fed to the reservoir, a high-dimensional dynamical system with internal variables $\mathbf{r} \in \mathbb{R}^M$, where M is the size of the reservoir. Here, following [17, 19], we implement the reservoir as

$$\mathbf{r}(t + \Delta t) = \tanh[\mathbf{A}\mathbf{r}(t) + \mathbf{W}_{\text{in}}\hat{\mathbf{x}}(t) + 1], \quad (3)$$

where the $M \times M$ matrix \mathbf{A} is a sparse matrix representing the internal structure of the reservoir network and the $M \times N$ matrix \mathbf{W}_{in} is a fixed input matrix. The reservoir output \mathbf{u} is constructed from the internal states as $\mathbf{u} = \mathbf{W}_{\text{out}}\mathbf{r}$, where the $N \times M$ output matrix \mathbf{W}_{out} is chosen so that \mathbf{u} approximates as best as possible the known training forcing function $\mathbf{f}(t)$. The optimization can be done by minimizing the cost function

$$\sum_{n=0}^{T/\Delta t} \|\mathbf{f}(-n\Delta t) - \mathbf{u}(-n\Delta t)\|^2 + \lambda \text{Tr}(\mathbf{W}_{\text{out}}\mathbf{W}_{\text{out}}^T) \quad (4)$$

via a ridge regression procedure, where the constant $\lambda \geq 0$ prevents over-fitting. With this procedure, the reservoir is trained to identify the forcing function $\mathbf{f}(t)$ given the observed values of $\hat{\mathbf{x}}(t)$. The reservoir can then be presented with a time series of the observed variables taken from (1), i.e., it can be evolved as

$$\mathbf{r}(t + \Delta t) = \tanh[\mathbf{A}\mathbf{r}(t) + \mathbf{W}_{\text{in}}\mathbf{x}(t) + 1]. \quad (5)$$

The reservoir output $\mathbf{u}(t) = \mathbf{W}_{\text{out}}\mathbf{r}$ will be, if the method is successful, a good approximation to the unknown disturbance, $\mathbf{u} \approx \mathbf{g}$. As we will see, the reservoir robustly identifies disturbances it has not observed previously. Fig. 1 illustrates our procedure in the training phase (top row) and recovery phase (bottom row).

In our examples, the reservoir matrix \mathbf{A} is a random matrix of size $M = 1000$ where each entry is uniformly distributed in $[-0.5, 0.5]$ with probability $6/M$ and 0 otherwise, and rescaled so that its spectral radius is 1.2. The input matrix \mathbf{W}_{in} is a random matrix where each entry is uniformly distributed in $[-0.01, 0.01]$. The ridge regression regularization constant is $\lambda = 10^{-6}$. We train the reservoir for $T = 150$ time units and use Euler’s method to solve the differential equations with a time step $\Delta t = 0.002$.

We demonstrate our method with both numerical simulations and experiments. For the numerical simulations, we consider a system where the intrinsic dynamics are given by the Lorenz system [28], i.e., system (1) is

$$\dot{x} = \sigma(y - x) + g_x(t), \quad (6)$$

$$\dot{y} = x(\rho - z) - y + g_y(t), \quad (7)$$

$$\dot{z} = xy - \beta z + g_z(t), \quad (8)$$

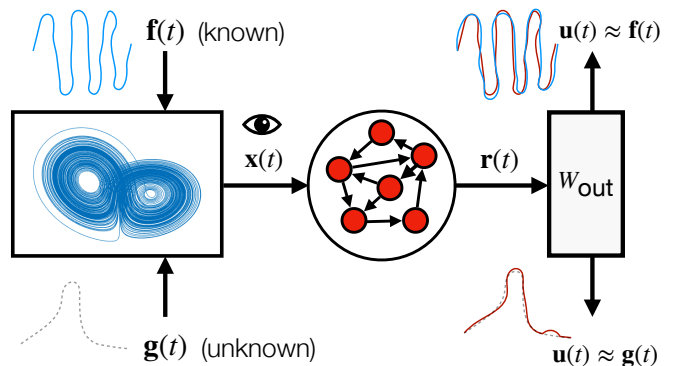


FIG. 1: Schematic illustration of our method. In the training phase (top row), a nonlinear system is forced with a training function $\mathbf{f}(t)$. Observations of the forced system are used to train a reservoir to approximate the training function. The reservoir subsequently identifies unknown disturbance functions (bottom row).

with $\rho = 28$, $\sigma = 10$, and $\beta = 8/3$. For the unknown disturbance we consider two examples: (i) a deterministic forcing $[g_x, g_y, g_z]^T = [x_R/10, y_R/10, 0]^T$, where $x_R(t)$ and $y_R(t)$ are the x and y coordinates of an auxiliary Rössler system [29] (assumed to be unknown), $\dot{x}_R = -y_R - z_R$, $\dot{y}_R = x_R + ay_R$, $\dot{z}_R = b + z_R(x_R - c)$, with $a = 0.2$, $b = 0.2$, and $c = 5.7$, and (ii) a stochastic forcing $[g_x, g_y, 0]^T$ where both g_x and g_y satisfy the Langevin equation $dg/dt = -g/2 + \eta(t)$, where η is a white noise term satisfying $\langle \eta(t)\eta(t') \rangle = 2D\delta(t - t')$, with $D = 1.25$. In Fig. 2 we show the performance of the reservoir in recovering the unknown disturbance for different choices of training forcing function $[f_x(t), f_y(t), 0]^T$. (For simplicity of visualization we assume it is known that the forcing in the z coordinate is zero). Along the top row, i.e., panels (a)–(c), we plot the trajectory of the unknown disturbance functions $([x_R(t)/10, y_R(t)/10]^T$ in panels (a)–(b) and the stochastic forcing $[g_x, g_y, 0]^T$ in panel (c)) to be reconstructed (black curve), the reconstructed disturbances $[u_x(t), u_y(t)]^T$ (red curve), and the training forcing functions $[f_x(t), f_y(t)]^T$ (thick blue curves and symbols). For ease of visualization, Fig. 2(c) only shows the last 1/8 portion of the time-series.) From left to right we have trained the reservoirs with forcing functions consisting of a sine/cosine pair $[f_x(t), f_y(t)]^T = [\cos(0.05t), \sin(0.05t)]^T$, a slightly offset pair of cosine functions $[f_x(t), f_y(t)]^T = [\cos(0.05t), \cos(0.05t - 0.05)]^T$, and piecewise constant functions $[f_x(t), f_y(t)]^T = [\text{sign}(\cos(0.05t)), \text{sign}(\sin(0.05t))]^T$. Time series for the unknown and recovered disturbances, $g_y(t)$ and $u_y(t)$, are compared in the bottom row, (e)–(g), plotted in solid black and dashed red, respectively.

Remarkably, our results show that the reservoir can identify a chaotic or stochastic forcing function to the Lorenz system even when it was trained with a periodic function [Fig. 2(a)], or a piecewise constant function with only *four* different values [Fig. 2(c)]. [In fact, as we will

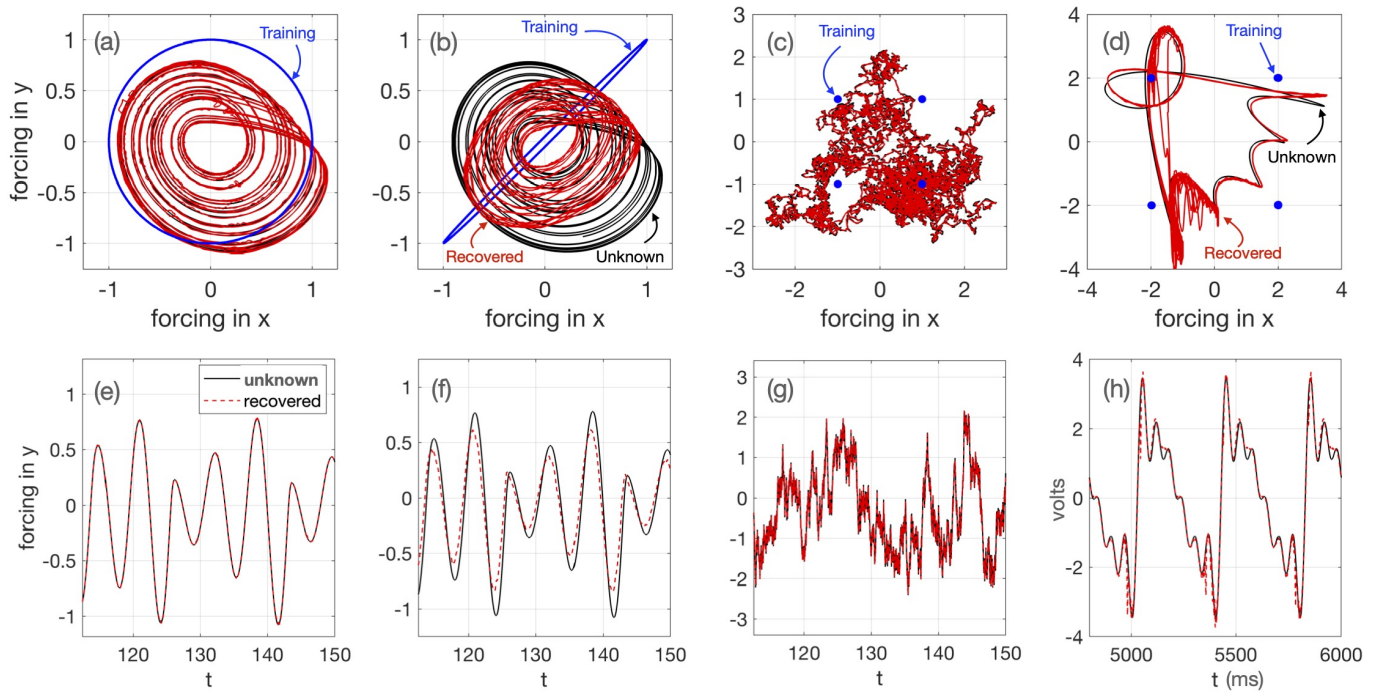


FIG. 2: (Top) Unknown and reconstructed disturbance functions $[g_x(t), g_y(t)]$ (black curve) and $[u_x(t), u_y(t)]$ (red curve) along with the training forcing functions $[f_x(t), f_y(t)]$ (thick blue curves and symbols). For each case the reservoir was trained with (a) $[f_x(t), f_y(t)] = [\cos(0.05t), \sin(0.05t)]$, (b) $[f_x(t), f_y(t)] = [\cos(0.05t), \cos(0.05t - 0.05)]$, (c) $[f_x(t), f_y(t)] = [\text{sign}(\cos(0.05t)), \text{sign}(\sin(0.05t))]$, and (d) a harmonic function (see Supplemental Material). (Bottom) Time series for the unknown (solid black) and recovered (dashed red) disturbance functions in the y component, $g_y(t)$ and $u_y(t)$. Panels (d) and (h) were produced from experimental data.

discuss below and is shown in the Supplemental Material (SM), only three different values are needed]. Figure 2(b) illustrates the limitations on the forcing functions used to train the reservoir. In this example, the forcing functions satisfy $f_x \approx f_y$. Given this limited training, the reservoir has trouble extrapolating to functions away from the manifold $f_x = f_y$, and the reconstruction of the disturbance suffers.

In addition to the numerical simulations, we tested our method on an experimental realization of the Lorenz system. An analog electric circuit which reproduces the dynamics of the Lorenz equations was built following Ref. [30] (see Supplemental Material). Function generators were used to introduce various types of additive forcing terms in both the x and y variables as in Eqs. (6)-(7). In the example shown in Figs. 2(d), (h), the circuit variables x , y , and z were sampled at a rate of 10 kHz for 20 seconds when forced with a pair of offset square waves with a frequency of 0.5 Hz. After training the reservoir as described above, the circuit was forced with a pair of offset harmonic functions (see Supplemental Material for details), the time series sampled as before, and the trained reservoir used to identify the forcing. Figure 2(d) shows the piecewise constant training forcing functions $(f_x(t), f_y(t))$ (blue symbols), the harmonic disturbance $(g_x(t), g_y(t))$ (black curve), and the recovered disturbance (red curve). To alleviate noise effects, the

recovered disturbance is a moving average of the reservoir prediction with a window of 20ms. Time series for the disturbance $f_y(t)$ (black curve) and the noise-filtered recovered disturbance (dashed red curve) are shown in Fig. 2(h). Despite some noise, the reservoir does a good job in recovering the disturbance. (The disturbance in the x component was also recovered with slightly better quality.) Additional examples are presented in the Supplemental Material.

An important question is what training forcing function \mathbf{f} should one use in order to recover an *a priori* unknown disturbance \mathbf{g} . In our numerical experiments, We have found that the reservoir computer is able to identify disturbances with range in a region approximately 5 times larger than the convex hull of the set $\{\mathbf{f}(-n\Delta t)\}_{n=0}^{T/\Delta t}$, with the same center. This condition is very mild; in addition to the training forcing functions shown in Fig. 2(a) and (b), we have successfully used, for example, a piecewise constant function with only *three values*. For these and other examples and additional discussion, see the Supplemental Material. Intuitively, if the range of the training forcing function \mathbf{f} does not contain enough information for the reservoir computer to extrapolate and infer the disturbance, the process will fail. In this Letter we have not attempted a rigorous or more general analysis of the conditions that training forcing functions should satisfy, and leave this for future

research. In addition to the example above where the unknown disturbance is chaotic, we have also successfully identified temporally localized, constant, periodic, and slowly varying, non-oscillatory forcing functions $\mathbf{g}(t)$ (see the Supplemental Material).

Suppression of the disturbance. Now we consider the problem of suppressing the undesired disturbance function $\mathbf{g}(t)$ with the aim of recovering the approximate undisturbed dynamics $d\mathbf{x}/dt = \mathbf{F}(\mathbf{x})$. For this we assume that the procedure described above has been successful, and that $\mathbf{u}(t) = W_{\text{out}}\mathbf{r}$ approximates the forcing to the system. We motivate our subsequent method by first considering a scheme where Eq. (1) is modified to

$$\frac{d\mathbf{x}}{dt} = \mathbf{F}(\mathbf{x}) + \mathbf{g}(t) - \alpha\mathbf{u}(t), \quad (9)$$

where α is the control gain, and \mathbf{u} is obtained by feeding \mathbf{x} to the trained reservoir. We refer to this scheme as the *simple control* scheme. Since the reservoir was trained to identify the forcing, in principle we have a self-consistent relationship

$$\mathbf{u} \approx \mathbf{g} - \alpha\mathbf{u}, \quad (10)$$

with solution

$$\mathbf{u}(t) \approx \frac{\mathbf{g}(t)}{1 + \alpha}. \quad (11)$$

The effective forcing $\mathbf{g}(t) - \alpha\mathbf{u}(t)$ in Eq. (9) reduces to $\mathbf{g}(t)/(1 + \alpha)$. In principle, then, choosing $\alpha \gg 1$ suppresses the forcing. However, this control scheme becomes unstable for moderate values of α . To understand this, we assume momentarily that \mathbf{g} is constant, and study the stability of the control scheme. On a given time step, the reservoir tries to approximate the forcing in Eq. (9), which is based on the previous reservoir output. Therefore, Eq. (10) needs to be treated as a dynamical system. A first approximation is

$$\mathbf{u}(t + \Delta t) \approx \mathbf{g} - \alpha\mathbf{u}(t), \quad (12)$$

which assumes that the reservoir approximates its own output at the previous time. In reality, the right-hand side of Eq. (12) might depend on previous history. Therefore, we regard Eq. (12) as a rough approximation to guide us in constructing a useful control scheme. Under Eq. (12), the fixed point (11), and therefore the control scheme, becomes unstable for $\alpha > 1$. In our example, we find numerically that the scheme becomes unstable at $\alpha \approx 2.5$, presumably due to the fact that Eq. (12) is only an approximation. Additional tests using non-constant \mathbf{g} (not shown) show the same behavior.

In order to create a more robust control scheme, we modify (9) to

$$\frac{d\mathbf{x}}{dt} = \mathbf{F}(\mathbf{x}) + \mathbf{g}(t) - \alpha\mathbf{v}(t), \quad (13)$$

$$\frac{d\mathbf{v}}{dt} = \frac{1}{\tau}(\mathbf{u} - \mathbf{v}), \quad (14)$$

where τ is a control parameter. We refer to this scheme as the *delayed control* scheme, since \mathbf{v} represents an exponentially weighted average of the previous values of \mathbf{u} . Now we repeat our previous approximation to this scheme. If, for example, the dynamics are solved using Euler's method, Eq. (12) now becomes

$$\mathbf{u}(t + \Delta t) \approx \mathbf{g} - \alpha\mathbf{v}(t), \quad (15)$$

$$\mathbf{v}(t + \Delta t) \approx \mathbf{v}(t) + \frac{\Delta t}{\tau}[\mathbf{u}(t) - \mathbf{v}(t)]. \quad (16)$$

Again assuming constant \mathbf{g} , a linear stability analysis shows that when $\tau/\Delta t > 1$ the fixed point $\mathbf{u} = \mathbf{v} = \mathbf{g}/(1 + \alpha)$ is linearly stable as long as $\alpha < \tau/\Delta t$. While we don't expect this estimate to be exact, we expect that the range of values of α for which the control scheme is stable will be greatly expanded when $\tau/\Delta t$ is large. Interestingly, in contrast to typical control problems, the presence of delays increases the stability of the control scheme. In summary, the delayed control algorithm for suppressing a disturbance $\mathbf{g}(t)$ is as follows: (i) Force the system with a known training forcing function \mathbf{f} , and train a reservoir computer so that its output \mathbf{u} approximates \mathbf{f} based on observations of the state variables $\hat{\mathbf{x}}$. (ii) Add a term $-\alpha\mathbf{v}$ to the disturbed system, where \mathbf{v} satisfies Eq. (14) with large τ .

We demonstrate our method with the same examples we used above, i.e., (i) a Lorenz system forced by a Rössler system as in Eqs. (6)-(8), where $[g_x, g_y, g_z]^T = [50x_R, 50y_R, 0]^T$ and (ii) a Lorenz system forced by a stochastic forcing $[g_x, g_y, 0]^T$ where both g_x and g_y satisfy the Langevin equation $dg/dt = -g/2 + \eta(t)$, where η is a white noise term satisfying $\langle \eta(t)\eta(t') \rangle = 2D\delta(t - t')$, with $D = 11.25$. (In order to illustrate the power of our method, the disturbance terms are chosen to be much larger than in the previous example.) After training the reservoir with the forcing $[f_x(t), f_y(t), f_z(t)]^T = [\cos(0.05t), \sin(0.05t), 0]^T$, we run the control scheme in Eqs. (13)-(14). In Fig. 3 we plot with blue curves (a) the deterministically disturbed Lorenz system without control [Eqs. (6)-(8)], (b) the stochastically disturbed Lorenz system without control, and (c) the deterministically disturbed Lorenz system with delayed control using $\alpha = 200$ and $\tau = 1$. [The stochastically disturbed Lorenz system with delayed control using $\alpha = 200$ looks qualitatively similar to (c) and is not shown.] For comparison, the undisturbed system is shown in orange. Without control [panels (a) and (b), blue], the Lorenz butterfly attractor is deformed by the strong disturbances. On the other hand, when delayed control is implemented [panel (c), blue], the difference with the undisturbed attractor (orange) can be made quite small. In order to quantify the difference between the controlled and original attractors, we solve Eqs. (6)-(8) with $g_x = g_y = g_z = 0$ for $T = 150$ time units using Euler's method with a timestep $\Delta t = 0.002$ after discarding a sizable transient and create a reference time series $\{\mathbf{x}_0(0), \mathbf{x}_0(\Delta t), \mathbf{x}_0(2\Delta t), \dots, \mathbf{x}_0(T/\Delta t)\}$ representing an approximation of the undisturbed attractor. Next, for

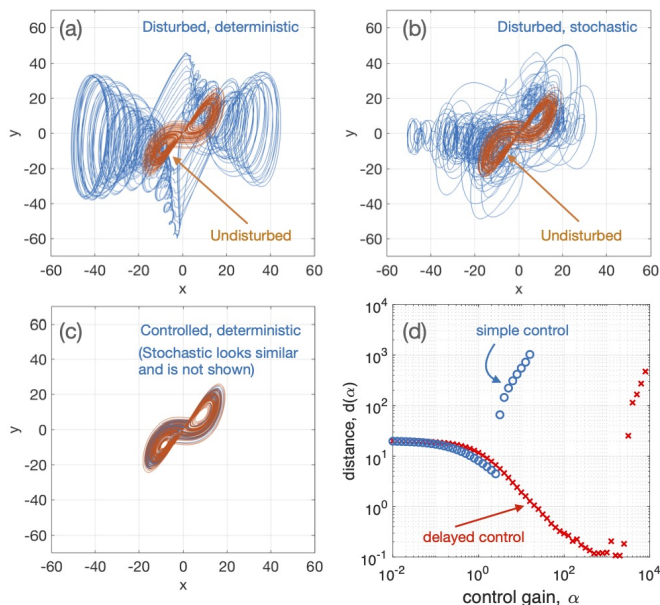


FIG. 3: (a) Deterministically disturbed attractor (blue). (b) Stochastically disturbed attractor (blue). (c) Deterministically disturbed attractor with the delayed control scheme using $\alpha = 200$ (blue). In (a)-(c), the orange curve shows the original, undisturbed Lorenz attractor. [The stochastically disturbed Lorenz system with delayed control using $\alpha = 200$ looks qualitatively similar to (c) and is not shown.] (d) Average distance between the controlled and original attractors, $d(\alpha)$, versus α for the simple control scheme (9) (blue circles) and the delayed control scheme (13)-(14) (red crosses).

a given value of α , again after discarding a transient, we compute a time series for the disturbed and controlled system, $\{\mathbf{x}(0), \mathbf{x}(\Delta t), \mathbf{x}(2\Delta t), \dots, \mathbf{x}(T/\Delta t)\}$. Then we compute the average distance between the points on the controlled trajectory and the reference time series as

$$d(\alpha) = \frac{1}{T/\Delta t} \sum_{i=0}^{T/\Delta t} \min_j \|\mathbf{x}(i\Delta t) - \mathbf{x}_0(j\Delta t)\|. \quad (17)$$

In Fig. 3(d) we plot the distance $d(\alpha)$ versus α for both

the simple control scheme (9) (blue circles) and for the delayed control scheme (13)-(14) (red crosses) for the deterministic disturbance. The simple control scheme reduces the error until it becomes unstable at approximately $\alpha \sim 2.5$. In contrast, the delayed control scheme reduces the error to very small levels for large values of α , before it also becomes unstable at approximately $\alpha \sim 2500$. (For both methods, the values of α for which no data are shown resulted in numerical instability.) In practice, a suitable value of α could be chosen either by comparing the controlled attractor to the undisturbed one, if it is available, or by choosing α large enough that the controlled attractor doesn't change appreciably when increasing α further, as it is often done with the time-step of numerical ODE solvers.

In summary, we have presented and demonstrated both numerically and experimentally a method that allows an unknown disturbance to an unknown dynamical system to be identified and suppressed in real-time, based only on previous observations of the system forced with a known forcing function. Our method is applicable, for example, to the problem of identifying node and line disturbances in networked dynamical systems such as power grids [7–9], and more broadly to the various fields where disturbances need to be suppressed in real-time [4]. While our method does not require knowledge of the underlying dynamics of the system, it requires one to be able to force it with the addition of a known training forcing function, and subsequently with the term $-\alpha\mathbf{v}$. The consideration of nonlinear disturbances is left for another manuscript [31]. In addition, we assumed that all the variables of the system can be observed. In principle, one could use our method by training the reservoir using an observed function $\mathbf{H}(\mathbf{x})$ of the state vector, but we have not explored this generalization. Another important research direction is to determine the class of appropriate training forcing functions, given a dynamical system and the anticipated characteristics of the disturbance.

ACKNOWLEDGMENTS

PSS acknowledges support from NSF grant MCB2126177. JGR acknowledges support from NSF Grant DMS-2205967.

-
- [1] Thomas R Nudell and Aranya Chakraborty. A graph-theoretic algorithm for disturbance localization in large power grids using residue estimation. In *2013 American Control Conference*, pages 3467–3472. IEEE, 2013.
 - [2] Swarnabala Upadhyaya and Sanjeeb Mohanty. Power quality disturbance localization using maximal overlap discrete wavelet transform. In *2015 Annual IEEE India Conference (INDICON)*, pages 1–6. IEEE, 2015.
 - [3] Abraham T Mathew and MN Aravind. Pmu based disturbance analysis and fault localization of a large grid using wavelets and list processing. In *2016 IEEE Region 10 Conference (TENCON)*, pages 879–883. IEEE, 2016.
 - [4] Wen-Hua Chen, Jun Yang, Lei Guo, and Shihua Li. Disturbance-observer-based control and related methods—an overview. *IEEE Transactions on industrial electronics*, 63(2):1083–1095, 2015.
 - [5] VH Ferreira, R Zanghi, MZ Fortes, GG Sotelo, R da Boa Morte Silva, JCS Souza, CHC Guimarães, and S Gomes Jr. A survey on intelligent system application to fault diagnosis in electric power system transmission

- lines. *Electric Power Systems Research*, 136:135–153, 2016.
- [6] Hyang-Won Lee, Jianan Zhang, and Eytan Modiano. Data-driven localization and estimation of disturbance in the interconnected power system. In *2018 IEEE International Conference on Communications, Control, and Computing Technologies for Smart Grids (SmartGridComm)*, pages 1–6. IEEE, 2018.
- [7] Defu Wang, Xiaojuan Wang, Yong Zhang, and Lei Jin. Detection of power grid disturbances and cyber-attacks based on machine learning. *Journal of information security and applications*, 46:42–52, 2019.
- [8] Robin Delabays, Laurent Pagnier, and Melvyn Tyloo. Locating line and node disturbances in networks of diffusively coupled dynamical agents. *New Journal of Physics*, 23(4):043037, 2021.
- [9] Robin Delabays, Laurent Pagnier, and Melvyn Tyloo. Locating fast-varying line disturbances with the frequency mismatch. *IFAC-PapersOnLine*, 55(13):270–275, 2022.
- [10] Gerard Meurant. *The ecology of natural disturbance and patch dynamics*. Academic press, 2012.
- [11] Corrado Battisti, Gianluca Poeta, and Giuliano Fanelli. An introduction to disturbance ecology. *Cham: Springer*, pages 13–29, 2016.
- [12] Thomas R Bewley and Sharon Liu. Optimal and robust control and estimation of linear paths to transition. *Journal of Fluid Mechanics*, 365:305–349, 1998.
- [13] Thomas R Bewley, Roger Temam, and Mohammed Ziane. A general framework for robust control in fluid mechanics. *Physica D: Nonlinear Phenomena*, 138(3-4):360–392, 2000.
- [14] Fabien Juillet, BJ McKeon, and Peter J Schmid. Experimental control of natural perturbations in channel flow. *Journal of fluid mechanics*, 752:296–309, 2014.
- [15] Jan Verbesselt, Rob Hyndman, Achim Zeileis, and Darius Culvenor. Phenological change detection while accounting for abrupt and gradual trends in satellite image time series. *Remote Sensing of Environment*, 114(12):2970–2980, 2010.
- [16] John C Canfield. *Active disturbance cancellation in nonlinear dynamical systems using neural networks*. University of New Hampshire, 2003.
- [17] Jaideep Pathak, Brian Hunt, Michelle Girvan, Zhixin Lu, and Edward Ott. Model-free prediction of large spatiotemporally chaotic systems from data: A reservoir computing approach. *Physical review letters*, 120(2):024102, 2018.
- [18] Keshav Srinivasan, Nolan Coble, Joy Hamlin, Thomas Antonsen, Edward Ott, and Michelle Girvan. Parallel machine learning for forecasting the dynamics of complex networks. *Physical Review Letters*, 128(16):164101, 2022.
- [19] Jaideep Pathak, Zhixin Lu, Brian R Hunt, Michelle Girvan, and Edward Ott. Using machine learning to replicate chaotic attractors and calculate lyapunov exponents from data. *Chaos: An Interdisciplinary Journal of Nonlinear Science*, 27(12):121102, 2017.
- [20] Daniel Canaday, Andrew Pomerance, and Daniel J Gauthier. Model-free control of dynamical systems with deep reservoir computing. *Journal of Physics: Complexity*, 2(3):035025, 2021.
- [21] Amitava Banerjee, Jaideep Pathak, Rajarshi Roy, Juan G Restrepo, and Edward Ott. Using machine learning to assess short term causal dependence and infer network links. *Chaos: An Interdisciplinary Journal of Nonlinear Science*, 29(12):121104, 2019.
- [22] Viktoras Pyragas and Kestutis Pyragas. Using reservoir computer to predict and prevent extreme events. *Physics Letters A*, 384(24):126591, 2020.
- [23] Ling-Wei Kong, Yang Weng, Bryan Glaz, Mulugeta Haile, and Ying-Cheng Lai. Reservoir computing as digital twins for nonlinear dynamical systems. *Chaos: An Interdisciplinary Journal of Nonlinear Science*, 33(3), 2023.
- [24] Dhruvit Patel and Edward Ott. Using machine learning to anticipate tipping points and extrapolate to post-tipping dynamics of non-stationary dynamical systems. *Chaos: An Interdisciplinary Journal of Nonlinear Science*, 33(2):023143, 2023.
- [25] Gouhei Tanaka, Toshiyuki Yamane, Jean Benoit Héroux, Ryosho Nakane, Naoki Kanazawa, Seiji Takeda, Hidetoshi Numata, Daiju Nakano, and Akira Hirose. Recent advances in physical reservoir computing: A review. *Neural Networks*, 115:100–123, 2019.
- [26] Kohei Nakajima and Ingo Fischer. *Reservoir computing*. Springer, 2021.
- [27] Swarnendu Mandal and Manish Dev Shrimali. Learning unidirectional coupling using an echo-state network. *Physical Review E*, 107(6):064205, 2023.
- [28] Edward N Lorenz. Deterministic nonperiodic flow. *Journal of atmospheric sciences*, 20(2):130–141, 1963.
- [29] Otto Roessler. An equation for continuous chaos. *Physics Letters A*, 57(5):397–398, 1976.
- [30] Paul Horowitz and Winfield Hill. *The Art of Electronics: The x Chapters*, volume 1. Cambridge University Press, Cambridge, 2020.
- [31] Per Sebastian Skardal and Juan G. Restrepo. Detecting disturbances in network-coupled dynamical systems with machine learning. *arXiv preprint arXiv:2307.12771*, 2023.

Supplemental Material for Suppressing unknown disturbances to dynamical systems using machine learning

Juan G. Restrepo,¹ Clayton P. Byers,² and Per Sebastian Skardal³

¹*Department of Applied Mathematics, University of Colorado at Boulder, Boulder, CO 80309, USA*

²*Department of Engineering, Trinity College, Hartford, CT, 06106, USA*

³*Department of Mathematics, Trinity College, Hartford, CT, 06106, USA*

In this Supplemental Material we describe the experimental implementation of our method. We also present additional experimental and numerical examples to those shown in the main text. We illustrate conditions under which training forcing functions succeed or fail in training the reservoir to reconstruct various disturbances. While our examples are only qualitative, they illustrate the main conditions on appropriate training forcing functions, and we hope they will be helpful in guiding future, more rigorous investigations.

EXPERIMENTAL IMPLEMENTATION

We constructed an analog electric circuit to replicate the Lorenz equations through three integrators and two multipliers, following the implementation described in Refs. [1, 2] and shown schematically in Figure S1(a). In this implementation, the variables x , y , and z are the voltages shown in the diagram in Fig. S1(a) and correspond to the respective variables in the Lorenz system scaled down by a factor of 10 (the equations the system models are modified accordingly for this scaling). The

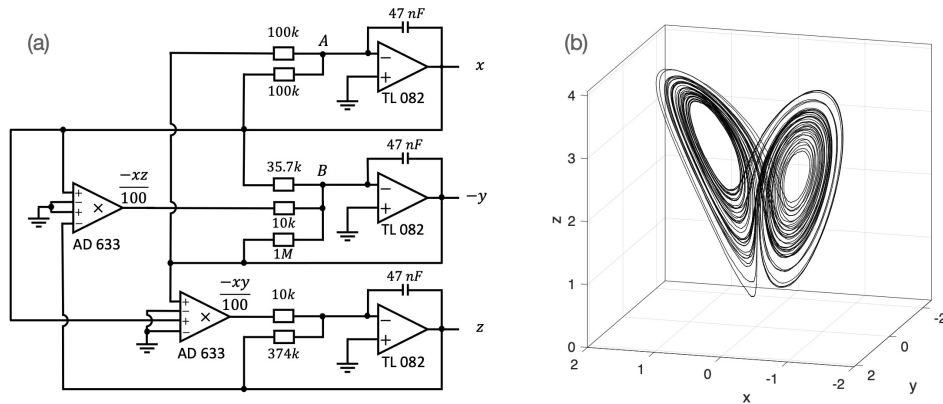


FIG. S1. Circuit for Lorenz attractor shown on the left. Integrators are based on the TL082 operational amplifier while the multipliers are based on the AD633 chip. Circuit recreated from [2]. Output of the circuit shown on the right, where units are in volts.

values used for the resistors are chosen to produce the appropriate coefficients in the Lorenz equations of $\sigma = 10$, $\beta = 8/3$, and $\rho = 28$. The integrating capacitors of 47 nF were chosen to provide oscillations on the order of 30 Hz. Resistors had a component tolerance of 1%, while the capacitors have a 5% tolerance. The multiplication was done with an AD633 analog multiplier, while the integrating circuit was based on an TL082 operational amplifier. The output of this circuit is shown in Fig. S1(b). The characteristic butterfly shape is readily apparent, with each output swinging around 4 volts peak to peak (Vpp). This analog circuit represents the “undisturbed system” described in the main text. While it is constructed to obey approximately the (scaled) Lorenz equations, the component tolerances make it, for practical purposes, and unknown system from which we can measure the state variables x , y , and z . Electronic noise adds an additional complication not present in our numerical simulations.

The external forcing is introduced into the circuit through the two points marked A and B in Figure S1(a). A function generator produces two signals at magnitudes that were approximately 4 Vpp to closely match the magnitude of the variables of the unforced circuit. These forcing signals were each passed through a unity gain buffer and a 1 MOhm resistor before being added to the signal at the input of the x and y integrators at A and B , respectively. The value of 1 MOhm allows the forcing signal to be of a comparable amplitude to the x , y , and z signals, and adds this function unscaled into the first two integrators.

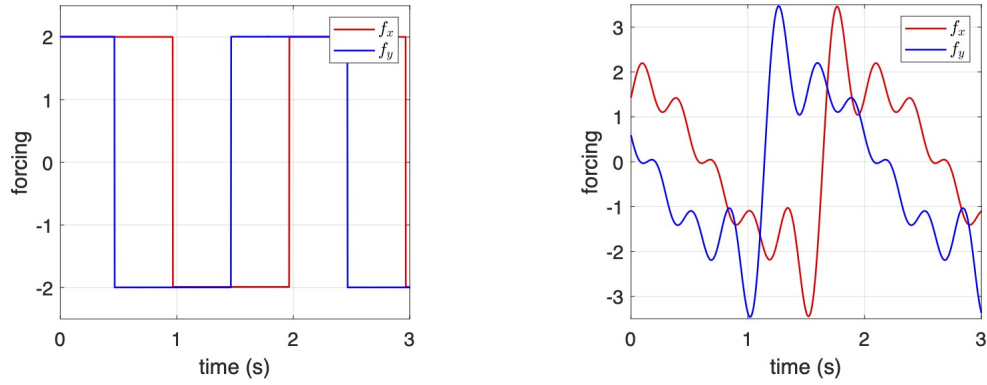


FIG. S2. (Left) Training forcing functions f_x (red) and $f_y(t)$ (blue). (Right) Disturbances to the x (red) and y (blue) components.

Experimental Example 1

In this example the circuit was forced with a pair of square waves of amplitude 2 Volts (4Vpp) with a frequency of 0.5 Hz and displaced 90 degrees. The disturbance to be identified was a harmonic function given by

$$f_x(t) = 0.63[3.16 \sin(\omega t) + \sin(2\omega t) + \sin(3\omega t) + \sin(4\omega t) + \sin(5\omega t) + \sin(6\omega t)] \quad (\text{S1})$$

where the fundamental frequency $\omega = \pi$ corresponds to 0.5 Hz, and with $f_y(t)$ displaced 90 degrees, i.e., $f_y(t) = f_x(t + (\pi/2)/\omega)$. The training forcing functions are shown in Fig. S2 (left), and the disturbances in Fig. S2 (right).

The circuit was forced with the training forcing functions above and x , y , z sampled at a rate of 10 kHz for 20 seconds. After training the reservoir with the time series thus produced, the disturbance was identified as described in the main text. Figure S3(a) shows the piecewise constant training forcing function (blue symbols), the unknown disturbance (black curve), the inferred disturbance (red curve), and the noise-filtered inferred disturbance (dark green curve). The noise-filtered inferred disturbance was obtained by applying a moving average to the reservoir output time series with an averaging window of 20 ms (200 data points). Figure S3(b) shows a portion of the time series for the y -components of the unknown disturbance (black curve), the inferred disturbance (red curve), and the noise-filtered inferred disturbance (dark green curve).

This example, part of which was shown in the main text, shows how the disturbance can be identified well even in the presence of experimental noise if the noise in the reservoir output is filtered.

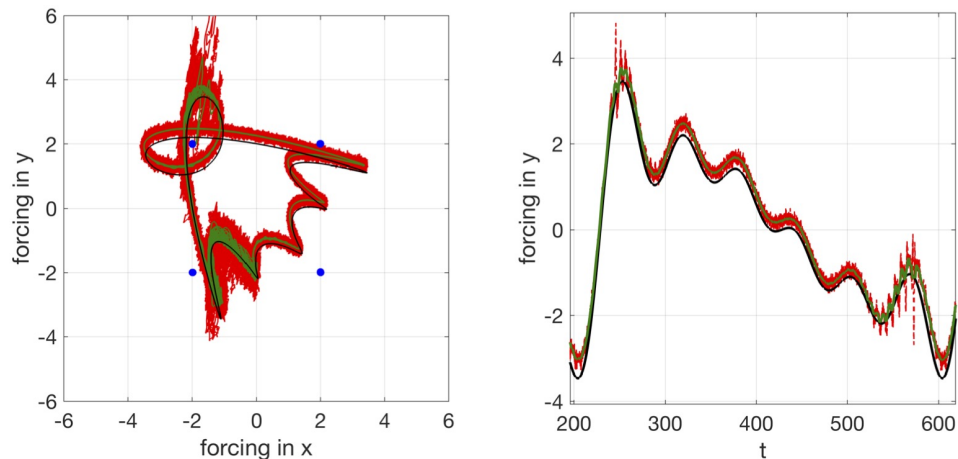


FIG. S3. (a) Training forcing function (blue symbols), unknown disturbance (black), inferred disturbance (red), and the noise-filtered inferred disturbance (dark green). (b) The y -components of the unknown disturbance (black curve), the inferred disturbance (red curve), and the noise-filtered inferred disturbance (dark green curve) as a function of time (in ms).

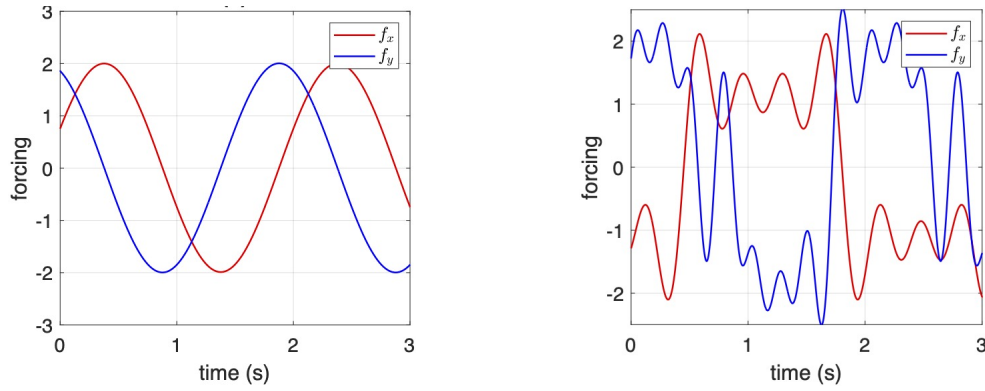


FIG. S4. (Left) Training forcing functions f_x (red) and $f_y(t)$ (blue). (Right) Disturbances to the x (red) and y (blue) components.

Experimental Example 2

Now we present an example where the circuit was forced with a pair of sine functions with amplitude 2 Volts (4Vpp) and a frequency of 0.5 Hz, with the forcing in the y component displaced 90 degrees from that in the x component, i.e., $f_x(t) = 2 \sin(\omega t)$, $f_y(t) = 2 \sin(\omega t + \pi/2)$, with $\omega = \pi$. The disturbance was a pair of even and odd harmonic functions given by

$$g_x(t) = 0.65[2.37 \sin(\omega_1 t) + \sin(3\omega_1 t) + \sin(5\omega_1 t) + \sin(7\omega_1 t)], \quad (\text{S2})$$

$$g_y(t) = 0.45[4 \sin(\omega_2 t) + \sin(2\omega_2 t) + 1.27 \sin(4\omega_2 t) + 1.27 \sin(6\omega_2 t) + 1.27 \sin(8\omega_2 t)] \quad (\text{S3})$$

where the fundamental frequencies $\omega_1 = 0.372\pi$ and $\omega_2 = \pi$ correspond to 0.37 and 0.5 Hz, respectively. The training forcing functions and the disturbances are shown in Fig. S4 (left) and (right), respectively. As before, Figure S5(a) shows the training forcing function (blue symbols), the unknown disturbance (black curve), the inferred disturbance (red curve), and the noise-filtered inferred disturbance (dark green curve). Figure S5(b) shows the y -components of the unknown disturbance (black curve), the inferred disturbance (red curve), and the noise-filtered inferred disturbance (dark green curve).

While the unfiltered, inferred disturbance (red curve) is very noisy, the noise-filtered version (dark green) does a good job in approximating the complex trajectory of the disturbance (black curve).

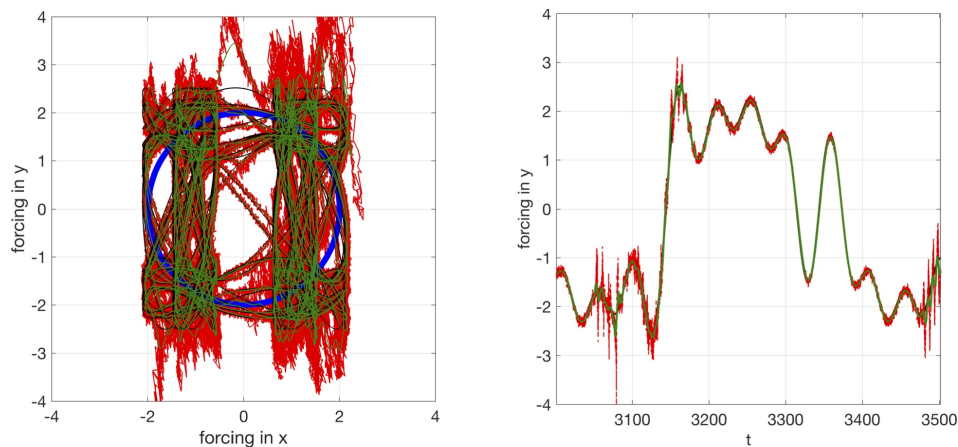


FIG. S5. (a) Training forcing function (blue symbols), unknown disturbance (black), inferred disturbance (red), and the noise-filtered inferred disturbance (dark green). (b) The y -components of the unknown disturbance (black curve), the inferred disturbance (red curve), and the noise-filtered inferred disturbance (dark green curve) as a function of time (in ms).

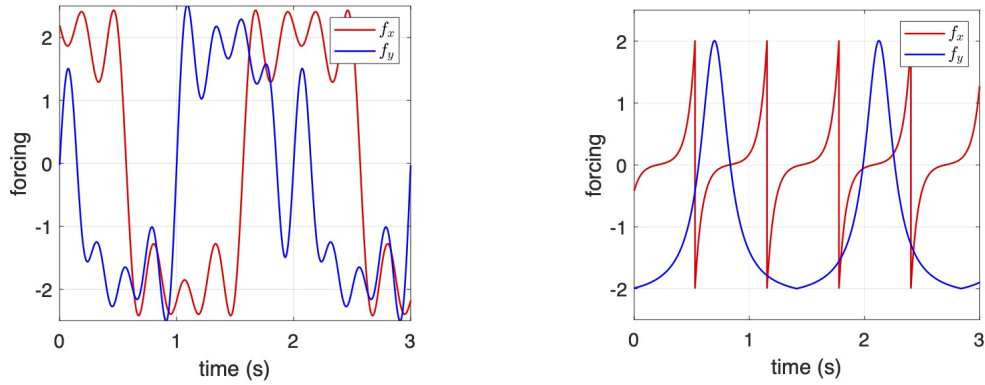


FIG. S6. (Left) Training forcing functions f_x (red) and $f_y(t)$ (blue). (Right) Disturbances to the x (red) and y (blue) components.

Experimental Example 3

Finally, in this example the training forcing in x and y were

$$g_x(t) = 0.6[3.95 \sin(\omega t) + \sin(3\omega t) + \sin(5\omega t) + \sin(7\omega t)], \quad (\text{S4})$$

$$g_y(t) = 0.45[4 \sin(\omega t) + \sin(2\omega t) + 1.27 \sin(4\omega t) + 1.27 \sin(6\omega t) + 1.27 \sin(8\omega t)], \quad (\text{S5})$$

where the fundamental frequency $\omega = \pi$ corresponds to 0.5 Hz. The disturbance in x was a truncated hyperbolic sine with a frequency of 1.6 Hz and amplitude of 4 Vpp. The disturbance in y was based on a truncated Cauchy distribution that repeated at 0.7 Hz with an amplitude of 4 Vpp. These are plotted in Figure S6. As before, Figure S7(a) shows the training forcing function (blue curve), the unknown disturbance (black curve), the inferred disturbance (red curve), and the noise-filtered inferred disturbance (dark green curve). Figure S5(b) shows the y -components of the unknown disturbance (black curve), the inferred disturbance (red curve), and the noise-filtered inferred disturbance (dark green curve). In this example the unfiltered inferred disturbance (red curves) is much more noisy than in the previous examples, probably because of the rapid swings in the disturbance functions. Nevertheless, after noise filtering the prediction of our method (dark green curves) recovers reasonably well the unknown disturbance (black curves).

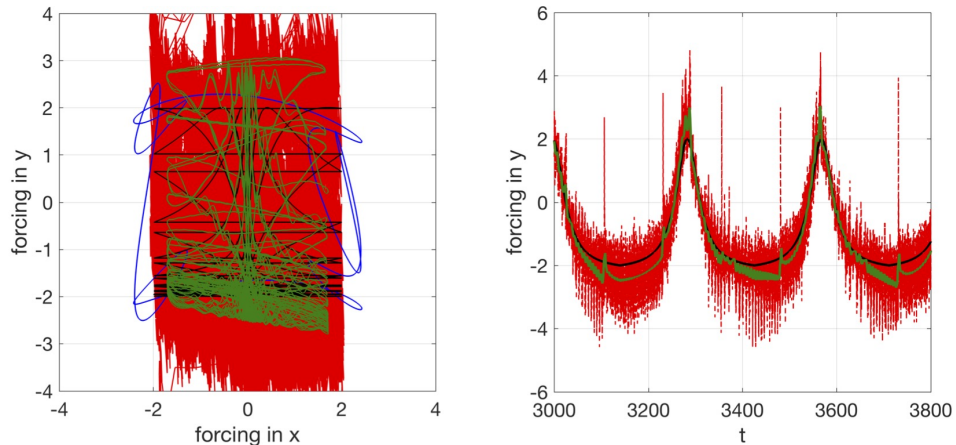


FIG. S7. (a) Training forcing function (blue symbols), unknown disturbance (black), inferred disturbance (red), and the noise-filtered inferred disturbance (dark green). (b) The y -components of the unknown disturbance (black curve), the inferred disturbance (red curve), and the noise-filtered inferred disturbance (dark green curve) as a function of time (in ms).

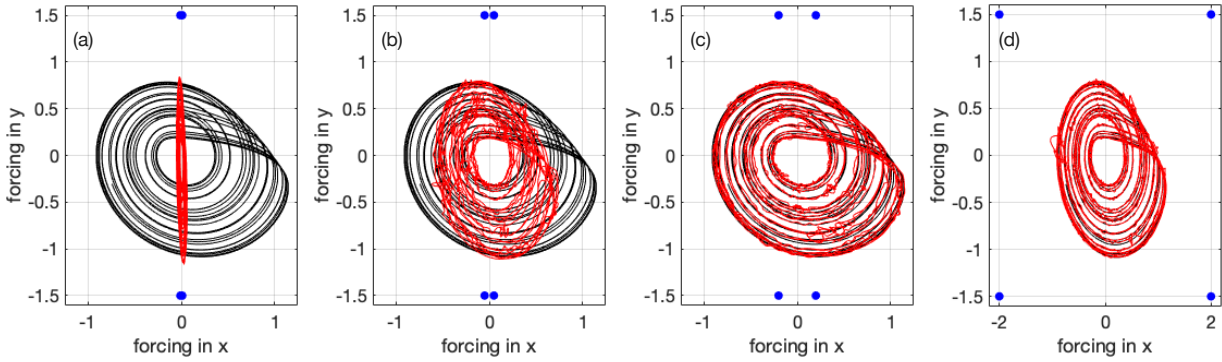


FIG. S8. Unknown disturbance (solid black curve), training forcing function (blue circles), and recovered disturbance (red curves). The training forcing functions are $[f_x(t), f_y(t), 0] = [a \times \text{sign}(\cos(t)), 1.5 \times \text{sign}(\sin(t))]$ with (a) $a = 0.01$, (b) $a = 0.05$, (c) $a = 0.02$, and (d) $a = 2$.

NUMERICAL EXAMPLES

Example 1: chaotic Lorenz system forced with the Rössler system

In this Section we revisit and expand our numerical example from the main text, a system where the intrinsic dynamics and disturbance are given by

$$\dot{x} = -\sigma(y - x) + g_x(t), \quad (\text{S6})$$

$$\dot{y} = x(\rho - z) - y + g_y(t), \quad (\text{S7})$$

$$\dot{z} = xy - \beta z + g_z(t), \quad (\text{S8})$$

with $\rho = 28$, $\sigma = 10$, and $\beta = 8/3$. In the examples below, $x_R(t)$, $y_R(t)$, and $z_R(t)$ are the x , y , and z coordinates of an auxiliary Rössler system, $\dot{x}_R = -y_R - z_R$, $\dot{y}_R = x_R + ay_R$, $\dot{z}_R = b + z_R(x_R - c)$, with $a = 0.2$, $b = 0.2$, and $c = 5.7$.

Piecewise constant training forcing function with rectangular convex hull

The unknown disturbance is taken to be $[g_x, g_y, g_z]^T = [x_R(t)/10, y_R(t)/10, 0]$. In Fig. S8 we show the performance of the reservoir in recovering the unknown disturbance for training forcing functions $[f_x(t), f_y(t), 0] = [a \times \text{sign}(\cos(t)), 1.5 \times \text{sign}(\sin(t))]$ for various values of a . In this case, the convex hull of the range of the training forcing function is the rectangle $[-a, a] \times [-1.5, 1.5]$. For small values of a , this rectangle does not extend sufficiently in the x direction to allow the reservoir to learn the dynamics in this direction. Consequently, the unknown disturbance is not recovered properly [panels (a) and (b)]. When the convex hull has enough extension in the x direction [panels (c) and (d)], the reservoir recovers the unknown disturbance satisfactorily.

Piecewise constant training forcing function with triangular convex hull

In this example we illustrate how three non-coaligned points, which generate a convex hull with finite volume, can be used as the range of the training force. The unknown disturbance is taken to be $[g_x, g_y, g_z]^T = [x_R(t)/10, y_R(t)/10, 0]$. In Fig. S9 we show the performance of the reservoir in recovering the unknown forcing for training forcing functions

$$[f_x(t), f_y(t), 0] = \begin{cases} c[\text{sign}(\cos(t)), \text{sign}(\sin(t))], & \sin(t) < 0, \\ c[\text{sign}(\cos(t)), 1], & \sin(t) > 0, \end{cases} \quad (\text{S9})$$

for $c = 0.02$ (a), $c = 0.05$ (b), $c = 0.2$ (c), and $c = 2$ (d). For small c [panels (a) and (b)], the convex hull of the training forcing function is not sufficiently large, and the reservoir has trouble extrapolating beyond the limited region that it explores during training. In contrast, for larger values of c [panels (c) and (d)], the reservoir can learn the unknown disturbance, even though it is in a region that was not explored during training.

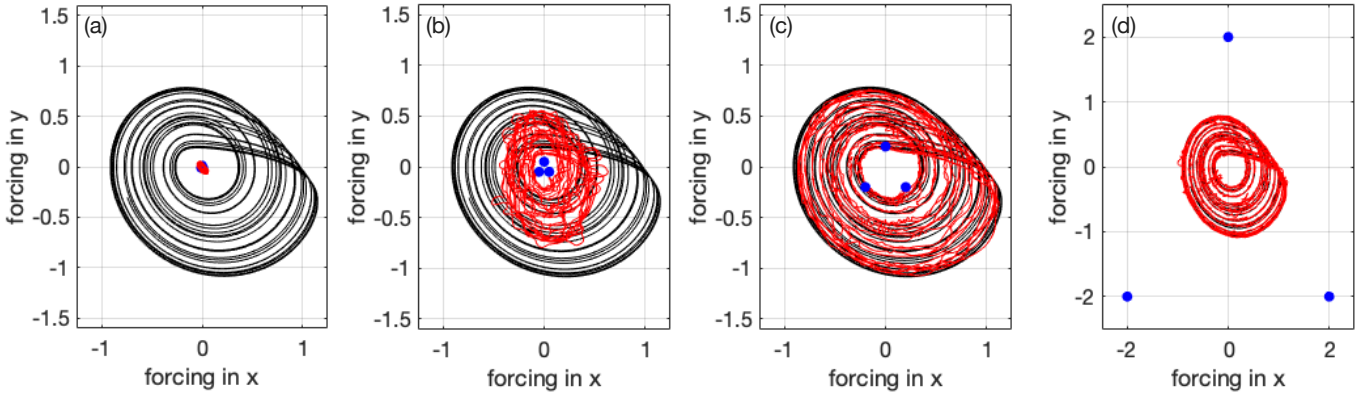


FIG. S9. Unknown disturbance (solid black curve), training forcing function (blue circles), and recovered disturbance (red curves). The training forcing functions are in Eq. (S9) with (a) $c = 0.01$, (b) $c = 0.05$, (c) $c = 0.2$, and (d) $c = 2$.

Training forcing function far away from the unknown disturbance

Here we illustrate what can happen when the range of the training forcing function is too far away from the range of the unknown disturbance. In the example below, the unknown disturbance is, again, $[g_x, g_y, g_z]^T = [x_R(t)/10, y_R(t)/10, 0]$. The training forcing function is $[f_x(t), f_y(t), 0] = [-b + 0.2 \cos(t/2), \sin(t/2), 0]$. Fig. S10 shows the result of using $b = 10$ (a), $b = 4$ (b), and $b = 1$ (c). For large b , the reservoir does not correctly reproduce the unknown disturbance.

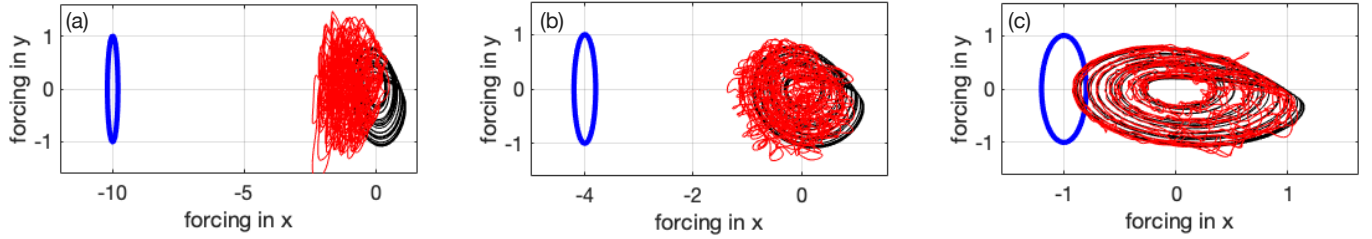


FIG. S10. Unknown disturbance (solid black curve), training forcing function (blue circles), and recovered disturbance (red curves). The training forcing functions are $[f_x(t), f_y(t), 0] = [-b + 0.2 \cos(t/2), \sin(t/2), 0]$ with (a) $b = 10$, (b) $b = 4$, and (c) $b = 1$.

Example 2: chaotic Lorenz system forced with other functions

Here we illustrate how our method allows us to identify unknown disturbances with different characteristics. In all the examples below, we use a training forcing function $[f_x(t), f_y(t), f_z(t)] = [\cos(t/2), 0, 0]$ and an unknown disturbance in the x coordinate only, $[g_x, g_y, g_z]^T = [g, 0, 0]$. Figure S11 shows the unknown disturbance $g(t)$ (solid black curves) and the inferred disturbance $u_x(t)$ (noisy red curves) for: (a) a temporally localized Gaussian disturbance, $g(x) = \exp(-(t - 75)^2/400)$; (b) a non-periodic, non-stationary signal, $g(x) = \sin(t^2/100) + 0.15t \sin(0.4t) + 1$; (c) an exponentially saturating signal $g(x) = 1 - \exp(-t/100)$; and (d) two short, temporally localized signals, $g(x) = H(t - 50) - H(t - 55) + H(t - 100) \exp(-(t - 100)/10)$, where $H(\cdot)$ is the Heaviside function.

Example 3: periodic Lorenz system

Finally, in this example we illustrate how our disturbance identification and suppression method also works when the original system is periodic. Here, we use the same system and parameters for Example 1, except for two parameters of the Lorenz system, $\rho = 160$ and $\beta = 6$. For these parameters the Lorenz system is periodic. We use the disturbance $[g_x, g_y, g_z]^T = [x_R(t)/10, y_R(t)/10, 0]$ and the training forcing function $[f_x(t), f_y(t), 0] = [\cos(0.05t), \sin(0.05t), 0]$. Fig. S12 shows the result of using the stable control scheme on this system with (a) $\alpha = 0$, (b) $\alpha = 10$, and (c) $\alpha = 200$. For large values of α , as expected, the dynamics of the disturbed and controlled system approximate closely the dynamics of the original system.

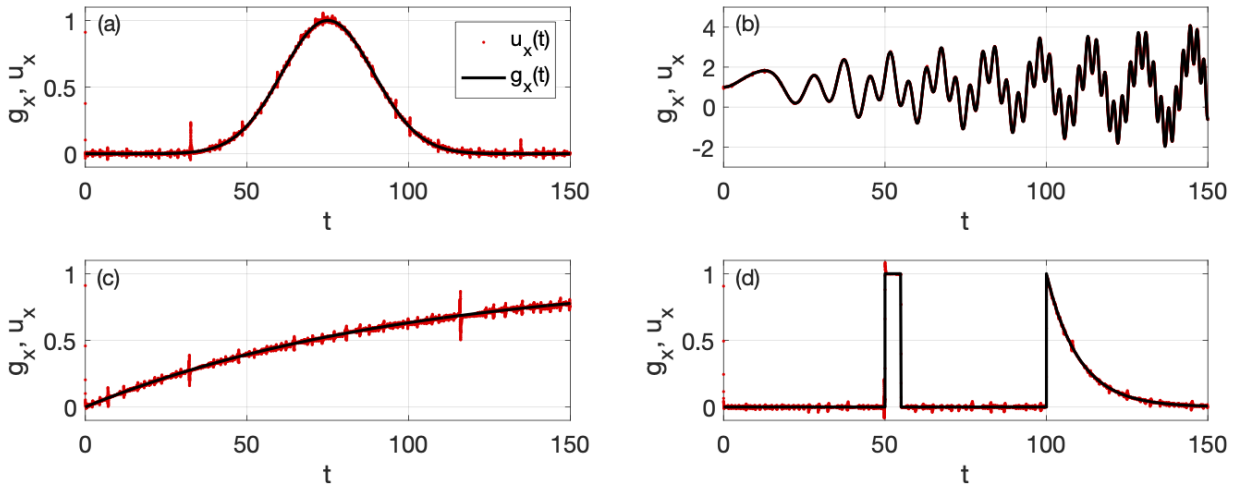


FIG. S11. Unknown disturbance $g(t)$ (solid black lines) and recovered disturbance $u(t)$ (red noisy lines) for (a) a temporally localized Gaussian disturbance, $g(x) = \exp(-(t - 75)^2/400)$; (b) a non-periodic, non-stationary signal, $g(x) = \sin(t^2/100) + 0.15t \sin(0.4t) + 1$; (c) an exponentially saturating signal $g(x) = 1 - \exp(-t/100)$; and (d) two short, temporally localized signals, $g(x) = H(t - 50) - H(t - 55) + H(t - 100) \exp(-(t - 100)/10)$.

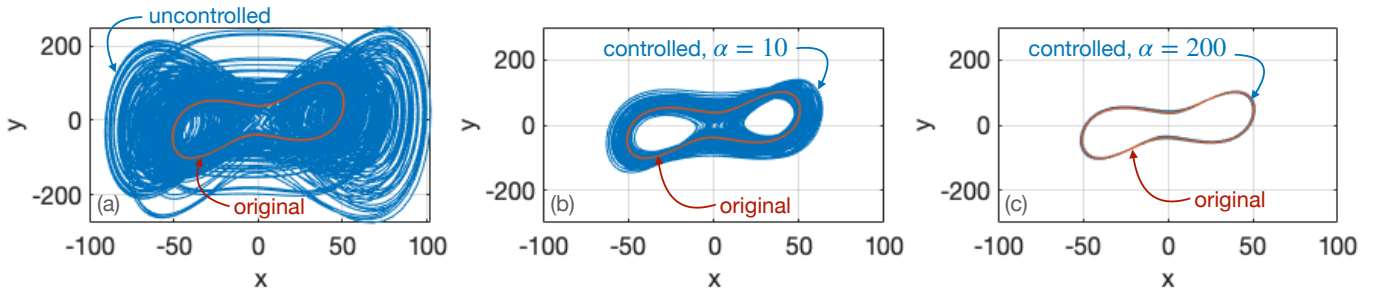


FIG. S12. (a) Uncontrolled, disturbed system (blue). (b) Disturbed attractor with the stable control scheme using $\alpha = 10$ (blue). (c) Disturbed attractor with the stable control scheme using $\alpha = 200$ (blue). In all plots, the orange curve shows the original, undisturbed Lorenz limit cycle.

- [1] Andrew L Fitch, Herbert HC Iu, and Dylan DC Lu. An analog computer for electronic engineering education. *IEEE Transactions on Education*, 54(4):550–557, 2010.
- [2] Paul Horowitz and Winfield Hill. *The Art of Electronics: The x Chapters*, volume 1. Cambridge University Press, Cambridge, 2020.